AD-A170 916 UPDATE OF ENDF/B-V MOD-3 IRON NEUTRON-PRODUCING REACTION CROSS SECTIONS A..(U) OAK RIDGE NATIONAL LAB TN C Y FU ET AL. JUL 86 ORNL/TM-9964 DE-AC05-840R21400 1/1

UNCLASSIFIED F/G 20/8 NL

END
DATE FILMED
9-86

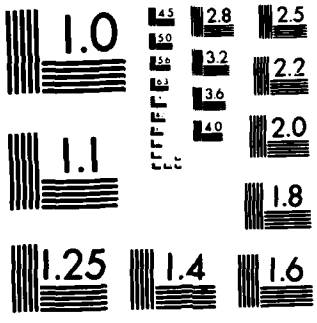

(12)

ornl

ORNL/TM-9964
ENDF-341

OAK RIDGE
NATIONAL
LABORATORY

MARTIN MARIETTA

Update of ENDF/B-V Mod-3 Iron: Neutron-Producing Reaction Cross Sections and Energy-Angle Correlations

C. Y. Fu
D. M. Hetrick

OPERATED BY
MARTIN MARIETTA ENERGY SYSTEMS, INC.
FOR THE UNITED STATES
DEPARTMENT OF ENERGY

Printed in the United States of America. Available from
National Technical Information Service
U.S. Department of Commerce
5285 Port Royal Road, Springfield, Virginia 22161
NTIS price codes—Printed Copy: A03; Microfiche A01

ORNL/TM-9964
ENDF-341

Engineering Physics and Mathematics Division

UPDATE OF ENDF/B-V MOD-3 IRON: NEUTRON-PRODUCING REACTION CROSS SECTIONS AND ENERGY-ANGLE CORRELATIONS

C. Y. Fu
D. M. Hetrick

Date of Issue: July 1986

Research Sponsored by
U.S. DOE Office of
Defense Nuclear Agency

Prepared by the
Oak Ridge National Laboratory
Oak Ridge, Tennessee 37831
operated by
Martin Marietta Energy Systems, Inc.
for the
U.S. DEPARTMENT OF ENERGY
under Contract No. DE-AC05-84OR21400

TABLE OF CONTENTS

UPDATE OF ENDF/B-V MOD-3 IRON: NEUTRON-PRODUCING REACTION CROSS SECTIONS AND ENERGY-ANGLE CORRELATIONS

ABSTRACT

An update of the ENDF/B-V Mod-3 evaluation for natural iron is described. The cross sections of (n,n') and $(n,2n)$ reactions are revised. Energy-angle correlations in the secondary (n,n') neutrons are introduced in the ENDF/B-V formats. Anisotropic angular distributions are provided for the secondary neutrons in $(n,2n)$, (n,np), and $(n,n\alpha)$ reactions. Relevant integral results, microscopic data, and nuclear model calculations that influence the revised results are summarized.

1. INTRODUCTION

This report describes an update of the ENDF/B-V Mod-3 evaluation (FU80, FU82) for natural iron (MAT 1326). The revised evaluation is referred to as MAT 1326 Mod-4. ENDF/B-V formats are used for this revision to meet the need for its immediate application.

The update, though motivated by results of integral studies (JO75, CR76) and applications, (MA85, PA85) is largely based on microscopic data and nuclear model calculations. The changes include inelastic scattering cross section for incident neutron energies (E_n) greater than 3 MeV, the entire $(n,2n)$ reaction cross section, and the energy-angle distributions in the secondary neutrons for $E_n > 4.6$ MeV. Most importantly, energy-angle correlations are introduced for the first time for the (n,n') secondary neutrons in the continuum. Anisotropic angular distributions (not energy-angle correlations) are also given for neutrons emitted in the $(n,2n)$, (n,np) and $(n,n\alpha)$ reactions.

As far as the above neutron-producing reactions are concerned, the ENDF/B-IV and ENDF/B-V Mod-1 evaluations for iron are nearly the same for $E_n > 3$ MeV (FU80), the energy range of the present work. Thus, the conclusions of neutron transport studies (JO75, CR76) based on ENDF/B-IV are as valid as those (MA85, PA85) based on ENDF/B-V Mod-1. These studies, summarized in Section 2, consistently indicate that the evaluated values for the (n,n') cross section are too large in a certain energy region. One result (JO75) attributes the underprediction of neutron penetration in thick iron to the isotropy assumption adopted for the (n,n') continuum (MT=91). Since neutrons emitted in (n,n') reaction tend to be forward peaked, the isotropy assumption would cause underprediction of neutron penetration and the effect would be similar to an overestimation of the total (n,n') cross section. Therefore, the lack of energy-angle correlation for the inelastically scattered neutrons in ENDF/B-IV and ENDF/B-V has to be part of the problem.

Modifications made for ENDF/B-V Mod-3, the starting point of the present revision, will cause some complications because the aforementioned integral studies and applications are based on either ENDF/B-IV or ENDF/B-V Mod-1. Two of the modifications for ENDF/B-V Mod-3 are relevant to the present work – one is the introduction of the cross sections of the ^{57}Fe inelastic levels, the other is a revision in the *(n,2n)* cross section (FU82). The ^{57}Fe inelastic cross section is small for $E_n > 3$ MeV, being about 1% of the total inelastic cross section at 5 MeV and being even smaller at higher energies. Therefore, the impact of the present revision on the inelastic cross section (approximately 10% at 5 MeV) is nearly the same on ENDF/B-IV, ENDF/B-V Mod-1, and ENDF/B-V Mod-3. The change in $(n,2n)$ cross section in Mod-3 is up to 10%, thus the present revision of $(n,2n)$ will be explicitly compared with both Mod-1 and Mod-3.

For these reasons, we will always designate the Mod number when we mention the $(n,2n)$ cross section. However, when we discuss the properties of a certain cross section that are nearly the same in Mod-1 and Mod-3, the Mod number may not always be mentioned.

An independent evaluation for natural iron for $E_n > 3$ MeV by Arthur and Young (AR80) of Los Alamos National Laboratory has smaller (n,n') cross sections than ENDF/B-V. The LANL evaluation is helpful for the present work but cannot replace it for the following reasons:

1. The present evaluation has uncertainty files ($MF=32$ and 33) and the LANL evaluation does not.
2. The present work is based on ENDF/B-V Mod-3 which has ^{57}Fe and the LANL work does not. The effect of ^{57}Fe on neutron attenuation has been shown to be significant in the keV region.(FU85)
3. The present evaluation contains energy-angle correlation (angular distribution as a function of E_n, E_n') for the inelastically scattered neutrons in the continuum (MT=91), not just anisotropic angular distribution (function of E_n) as in the LANL evaluation.

Two advances in the TNG code (FU87) since its application (FU75) for the ENDF/B-IV evaluation for iron make the code suitable for the present work. One is the inclusion of width-fluctuation correction for the continuum region, the other is the development of angular distribution capability in the precompound reaction which dominates high-energy particle emissions. Discussions of these theoretical advances and comparisons of calculated results with data are presented in Section 3.

Section 4 describes the method of representating energy-angle correlations in the ENDF/B-V format and the adjustments in other cross sections and uncertainty files due to the impact of the revised (n,n') and $(n,2n)$ cross sections. Section 5 contains a brief conclusion.

2. SUMMARY OF INTEGRAL RESULTS

Results of integral studies (JO75, CR76) and applications (MA85, PA85) of the ENDF/B-IV and ENDF/B-V Mod-1 cross-section sets of iron consistently indicate that the evaluated values of the (n,n') cross section are too large in a certain energy range and/or the energy-angle correlation (which has been assumed negligible in the evaluated files) in the inelastically scattered neutrons in the continuum is needed. These results dictate the direction of the present effort and are summarized below.

Johnson, Dorning, and Wehring (JO75) studied the neutron leakage spectra from an iron sphere (inner radius 7.65 cm, outer radius 38.10 cm) for two central sources. For a ^{252}Cf source, the ENDF/B-IV iron cross-section set underpredicts the neutron leakage spectrum for $E_n' < 6.5$ MeV by a factor of 2. For a D-T source, the calculated spectrum for $E_n' < 10$ MeV is too small by factors of 2 to 4. The authors suggest that the disagreement is partly due to the lack of realistic angular distributions of the direct component in the (n,n') reaction. This suggestion can now be interpreted more specifically in the light of our current understanding of nuclear reactions. In both ENDF/B-IV and ENDF/B-V, the inelastic scattering cross section is represented by 40 discrete levels up to 4.510 MeV and a continuum above. The cross sections of the discrete levels contain both direct and compound components and their angular distributions are adequate in our opinion. However, the angular distributions of inelastically scattered neutrons in the continuum were assumed isotropic. This assumption is far from adequate as can be seen from Fig. 1 in which double differential cross sections of iron for E_n = 14.5 MeV and E_n' = 2 to 10 MeV are shown. For outgoing neutron energies (E_n') greater than 4 MeV, the forward-peaking in the angular distributions is significant. In addition, it can also be seen from Fig. 1 that variations in the angular distributions with E_n' are rather large, i.e., there is a rather strong energy-angle correlation. Consequently, angular distributions for the (n,n') continuum have to be given as a function of E_n and E_n'; a task that has not been implemented in the ENDF/B-V system. We will discuss this problem further in Section 4. For now, it can be concluded that, if the forward-peaked angular distributions such as shown in Fig. 1 are represented in the cross-section files, the calculated neutron leakage spectra from the iron sphere will be increased. Therefore, one of the tasks of the present work is to calculate such angular distributions with the best nuclear model available, fit the calculated results to experimental data (which exist only at 14.5 and 25.7 MeV), and find a means to represent the calculated angular distributions as a function of E_n and E_n' within the confines of the current ENDF/B-V processing capability to facilitate immediate application of the new results.

Cramer and Oblow (CR76) carried out an analysis, based on ENDF/B-IV, of a neutron scattering experiment of a stepped iron ring 25.38 cm in outer diameter, 15.30 cm in inner diameter, and 3.72 cm thick. A detector was placed at the center of the ring, creating a scattering angle of 90 deg. with respect to the incident beam direction. Analytical and experimental data include integral count rates and pulse-height spectra as a function of E_n. From the results, we (not the authors of CR76) inferred that the (n,n') cross section for E_n = 3 to 5 MeV is too large and the $(n,2n)$ cross section for E_n = 14 to 15 MeV is also too large. A review of recent microscopic data, given in Section 3, appears to support these conclusions. Note that the ENDF/B-IV $(n,2n)$ cross section of iron is the same as that of ENDF/B-V Mod-1.

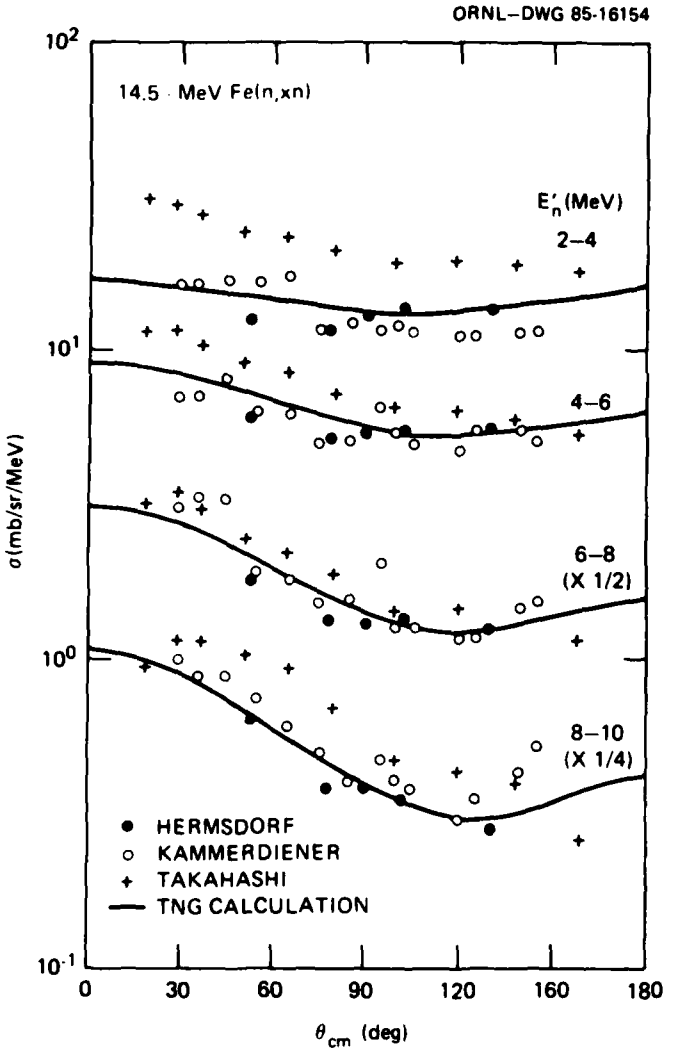

Fig. 1. Calculated and experimental double differential Fe(n,xn) cross sections for 14.5-MeV incident neutrons and several secondary energy ranges.

Maerker *et al.*, (MA85) in applying the LEPRICON methodology (a covariance reduction technique) to the analysis of the neutron fluences in the pressure vessel of an operating PWR power reactor, found that overall best agreement between a large body of calculated and experimental data, including those for standard neutron fields, can be achieved if the iron (n,n') cross section for E_n = 3 to 8 MeV is reduced by 8%. The energy range 3 to 8 MeV in this study was dictated by the covariance data given in the ENDF/B-V iron files in which the energy range 3 to 8 MeV for (n,n') is given as a fully-correlated group. Therefore, the conclusion here is not inconsistent with the energy range 3 to 5 MeV indicated in the result of Cramer and Oblow summarized above. Incidentally, the covariance group 3 to 8 MeV in the (n,n') covariance file may need to be broken up into two groups now that we realize the importance of this energy range in radiation damage studies.

Pace (PA85) attempted to reproduce the neutron dose rates in Hiroshima after the atomic bombing of that city by analyzing the activities in the sulphur samples found in the insulators in electric light poles. The calculated activities are too small and Pace attributes this observation to too large a (n,n') cross section for iron which was the major component in the bomb shell. For a $1/E$ neutron spectrum, most of the sulphur activities would come from neutrons of 3 to 5 MeV. Therefore, a reduction of the (n,n') cross section in the 3 to 8 MeV range, suggested by Maerker *et al.*, and a realistic representation of the energy-angle correlation in the inelastically scattered neutrons in the continuum, suggested by Johnson *et al.*, would also improve Pace's calculation.

3. MICROSCOPIC DATA AND NUCLEAR MODEL ANALYSIS

From the above discussions on the integral data, it is apparent that the energy-angle correlations in the inelastically scattered neutrons have to be given regardless of any changes in the total (n,n') and $(n,2n)$ cross sections. For this reason, we discuss the angular distributions first, then examine the total (n,n') and $(n,2n)$ cross sections.

Figures 1 and 2 display the double differential (n,xn) cross sections of iron at 14.5 and 25.7 MeV, respectively. The data are from KA72, HE75, MA83, TA83; the curves are the present calculation with the TNG code (preliminary accounts for most of the developments of this code can be found in FU75, FU76, FU79, FU81, FU84, FU86). Although the neutron energy of 25.7 MeV is outside the limit of the present purpose, the 25.7-MeV calculation shown in Fig. 2 is suggestive of the quality of the calculational tool in generating evaluated double differential cross sections.

Figure 3 shows the total inelastic cross section of iron from 3 to 20 MeV. The experimental data are from TH63, BE66, BR70, and SA72; the solid curve is the present evaluation (calculation for ^{56}Fe corrected for other small effects, see Section 4); and the dashed curve is ENDF/B-V Mod-3. Three observations should be made at this point:

1. The inelastic cross section below 3 MeV has resonance structures and the ENDF/B-V values were based on experimental data. Only revisions in the inelastic cross section for $E_n > 3$ MeV will be considered in this work.

2. From 3 to 5 MeV, the present calculation has been influenced by the integral results summarized in Section 2. However, for the energy range 3 to 7 MeV as a whole, the present calculation agrees well with the microscopic data. The average reduction of the present result between 3 and 8 MeV from that of ENDF/B-V is approximately 8%.

3. There is only one measurement (one data point) of the inelastic cross section of iron between 7 and 20 MeV. Determination of the cross-section shape in this energy range has to be based on nuclear model analysis with the aid of the most relevant data such as the nonelastic cross section and the 0.847-MeV gamma-ray production cross section. The inelastic cross section below 11 MeV is greater than 90% of the nonelastic cross section. The 0.847-MeV gamma-ray production cross section from threshold to 20 MeV, adjusted for isotopic abundance, is greater than 90% of the inelastic cross section. These relationships among the three cross sections are strongly defined by the code TNG which calculates all cross sections simultaneously with a consistent set of parameters.

The nonelastic cross section of iron from 3 to 20 MeV is shown in Fig. 4. The experimental data are from PH52, GR53, PA55, TA55, BE56, FL56, MA57, MA57, ST57, LE58, MA59, DE61; the solid curve is the present evaluation; the dashed curve is ENDF/B-V Mod-3. The data from 3 to 5 MeV are rather discrepant and do not help much in the determination of the inelastic cross section; however, we may consider the smallest data in Fig. 4 as lower limits. The data above 6 MeV are reasonably consistent; we do want the present calculation to agree with them.

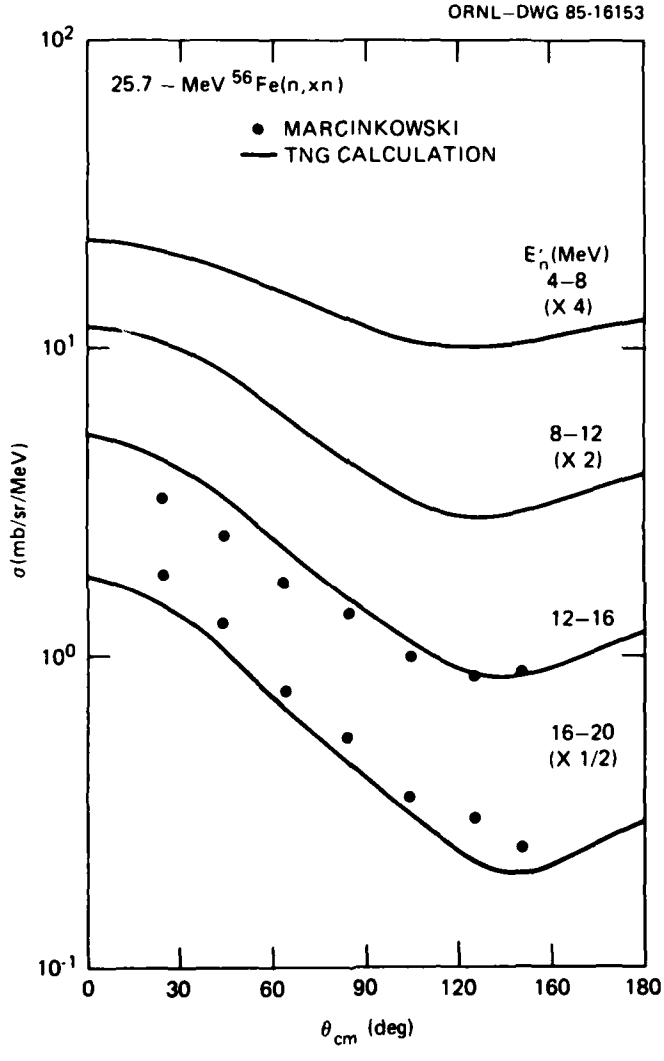

Fig. 2. Calculated and experimental double differential Fe(n,xn) cross sections for 25.7-MeV incident neutrons and several secondary energy ranges.

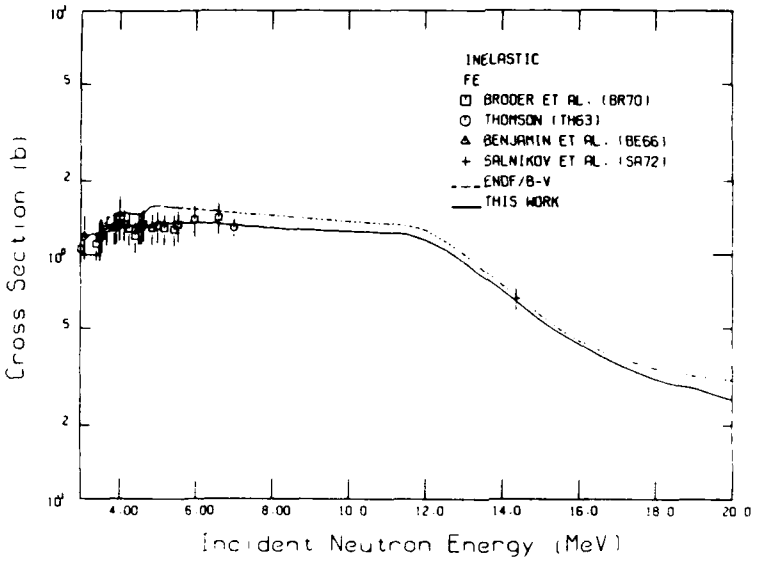

Fig. 3. Comparisons of the Fe inelastic cross sections of ENDF/B-V Mod-3 and this work with experimental data.

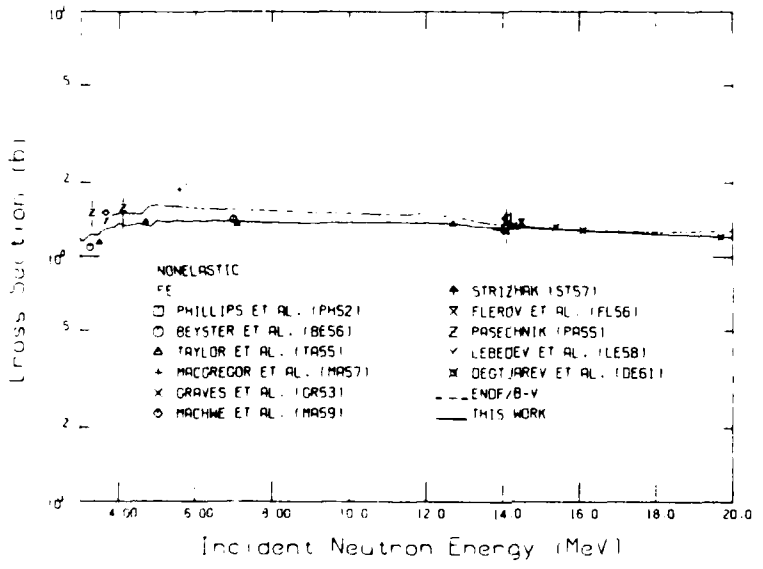

Fig. 4. Comparisons of the Fe nonelastic cross sections of ENDF/B-V Mod-3 and this work with experimental data.

The 0.847-MeV gamma-ray production cross section of iron from 3 to 20 MeV is shown in Fig. 5. The expeimental data are from BE66, BR67, RO68, BR70, DI72, CH74, LA74, BE75, OR75, LA85; the curve is the present calculation. The corresponding ENDF/B-V values for $E_n > 3$ MeV are given in continum distributions and cannot be retrieved accurately, hence not shown. The experimental data are all converted to elemental values. The calculation for ^{56}Fe has been multiplied by 0.918 (abundance of ^{56}Fe) to be consistent with the data. Some of the data were taken at 55 (or 125) degrees, others at 90 degrees. The former, after multiplied by 4 π, represents angle-integrated values well. The latter has to be multiplied by $1.125 \times 4\ \pi$. The factor, 1.125, was derived from the differential data of Lashkar *et al.* (LA74) at 2.5, 8.8, and 14.1 MeV. The 0.847-MeV gamma-ray production data from 7 to 20 MeV are the only indicator for the shape of the inelastic cross section in this energy range.

Now we turn to a brief discussion of the nuclear model calculation. From the microscopic data shown in Figs. 3 - 5 and the integral data summarized in Sect. 2, we conclude that the nuclear model analysis should at least satisfy the following two requirements:

1. The total inelastic cross section between 3 and 8 MeV in ENDF/B-V Mod-3 may be reduced, on the average, by up to 8% without disagreeing with the microscopic data.
2. The calculated nonelastic cross section and 0.847-MeV gamma-ray production cross section from 8 to 20 MeV should agree with the measurements.

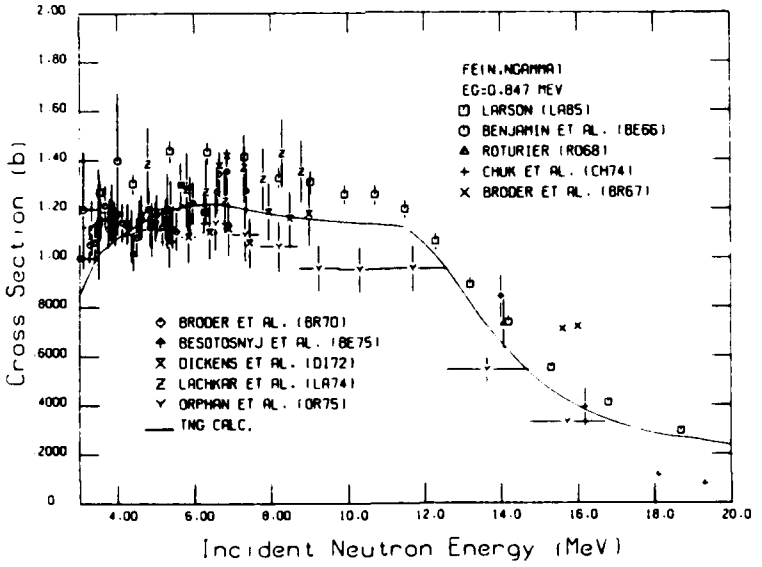

Fig. 5. Calculated and experimental production cross sections of the 0.847-MeV gamma rays from natural iron.

With these two goals in mind, it is relatively easy to explain the principal adjustment in the model parameters. The most important parameters in the present calculation are the optical model parameters which determine directly the nonelastic cross section above 8 MeV. At lower energies, the nonelastic cross section can be sensitive to the width-fluctuation correction and has to be calculated by both the optical model and the statistical model (as is done in the TNG code). In the calculation for ENDF/B-IV using an earlier version of the TNG code, the width-fluctuation correction had to be turned off for $E_n > 4.5$ MeV because the code did not have a capability for the correction for the continuum part. This capability has since been added. In the light of the present calculation, we conclude that the peak in the inelastic cross section near 5 MeV in the ENDF/B curve (see Fig. 3) is due to the lack of width-fluctuation correction at this energy. With this problem behind us, the principal effort in the present calculation is in the adjustment of the optical model parameters.

After trying several existing sets of optical model parameters, we found that the set given by Arthur and Young (AR80) gave the best overall results. However, some adjustment in the imaginary part of the optical model parameters were necessary to improve the fit to the nonelastic cross-section data from 3 to 20 MeV. The adjusted imaginary optical-model parameters are:

$$W_v = 0 \text{ , and}$$

$$W_s = 11.8 - 0.21E_n(MeV) \text{ ,}$$

where W_v is the volume part and W_s the surface part of the imaginary potential depth. There was another reason for this adjustment in addition to meeting the goals stated above. We found that we could not reproduce Arthur and Young's result for the nonelastic cross section from 3 to 7 MeV with their optical-model parameters. In this energy range, our calculated values for the nonelastic cross section are 20 to 70 mb lower than theirs. A plausible explanation for this difference is that they cut off the width-fluctuation correction between 4 and 5 MeV while we cut it off at 8 MeV. Our calculation, with the original Arthur and Young parameters, shows that there is still 50 mb reduction in the nonelastic cross section at 6 MeV due to the width-fluctuation correction. Therefore, part of the adjustment in the imaginary potential is to compensate for the missed width-fluctuation effect in Arthur and Young's calculation.

All other parameters are either taken from standard sources (level energies, Q-values, etc.) or have not been changed from earlier global analysis (proton and alpha-particle optical model parameters, precompound strength, etc., see FU79).

The $(n,2n)$ cross-section data for iron are shown in Fig. 6. The data are from AS58, WE62, SA72, QA77, CO78, VE79, FR80. The present calculation (solid curve) is somewhat better than ENDF/B-V Mod-1 (short dashed curve) but is comparable to Mod-3 (long dashed curve). The Mod-3 $(n,2n)$ cross section was taken from the Arthur and Young evaluation (AR80). The present calculation is for ^{56}Fe while some of the data are for natural iron.

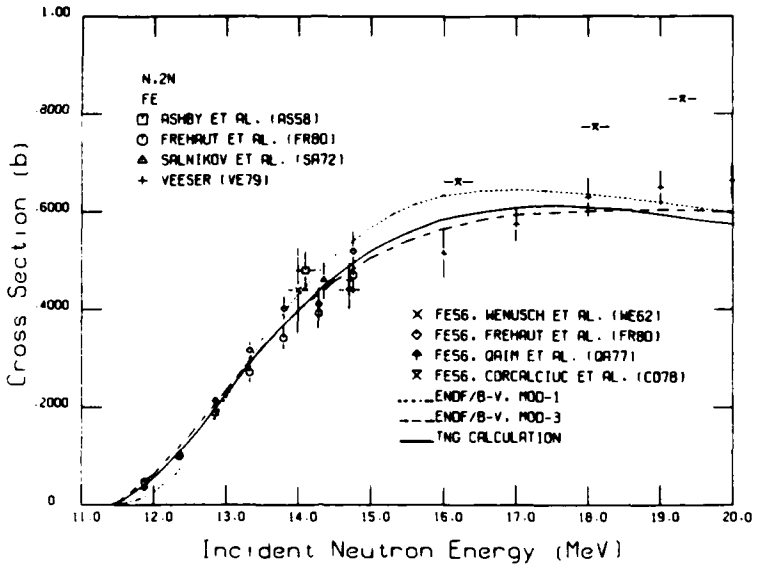

Fig. 6. Comparisons of the Fe(n,2n) cross sections of ENDF/B-V Mod-1, ENDF/B-V Mod-3, and the present calculation with measurements.

Except for the apparently erroneous data of CO78, the ^{56}Fe and natural iron (n,2n) cross-section data are in good agreement; thus no effort has been made to distinguish the two. The calculated ^{56}Fe (n,2n) cross section as shown in Fig. 6 has been adopted as the evaluated value for natural iron. The neutron, proton, and alpha-particle production spectra at E_n = 14.5 MeV are shown in Figs. 7 - 9, which are suggestive of good agreement of the present calculation with these data. The data are from CL72, HE75, HA77, GR79, and TA83.

From the presentation in this section, we can say that the present revision of the iron evaluation could not have been possible without the nuclear model analysis, particularly the inelastic cross section from 7 to 20 MeV and the energy-angular distributions in the secondary neutrons. The representation of such distributions with the ENDF/B-V format, with which the evaluated file can be processed readily, causes some complications which we discuss next.

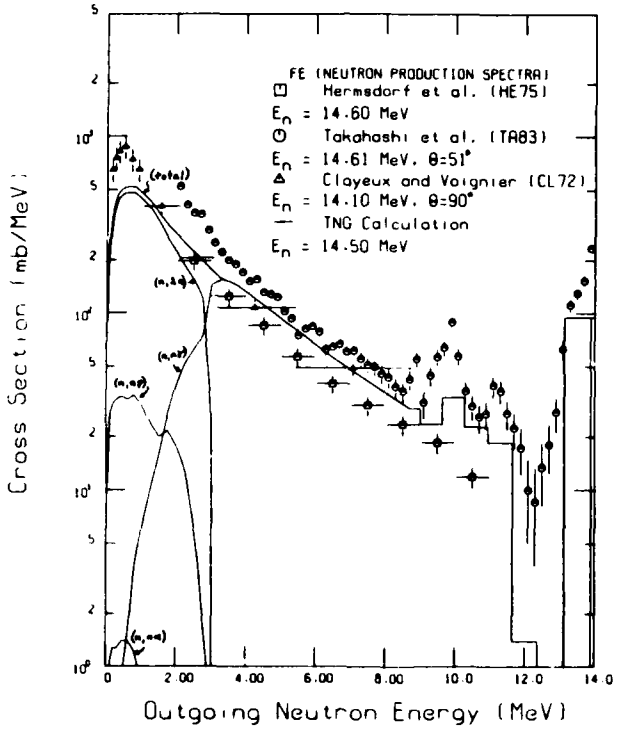

Fig. 7. Comparison of the neutron production spectrum of the present calculation with measurements. Various contributing components in the calculation are shown.

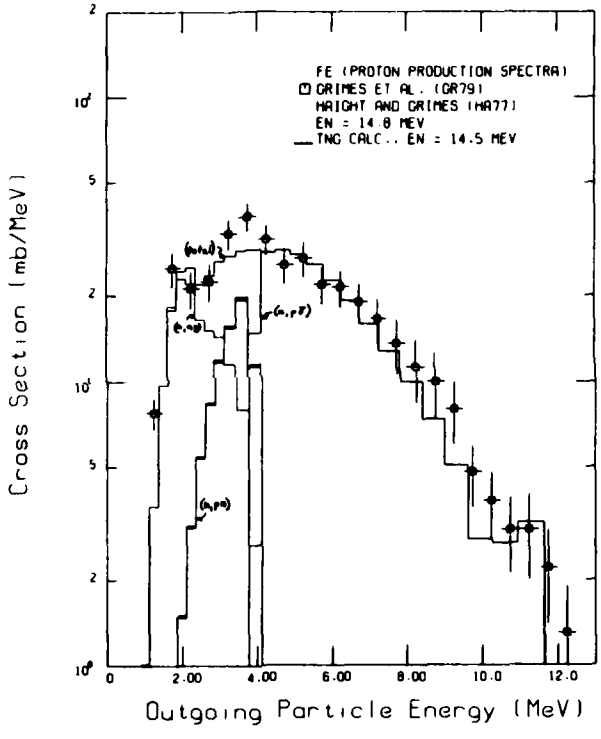

Fig. 8. Comparison of the proton production spectrum of the present calculation with measurements. Various contributing components in the calculation are shown.

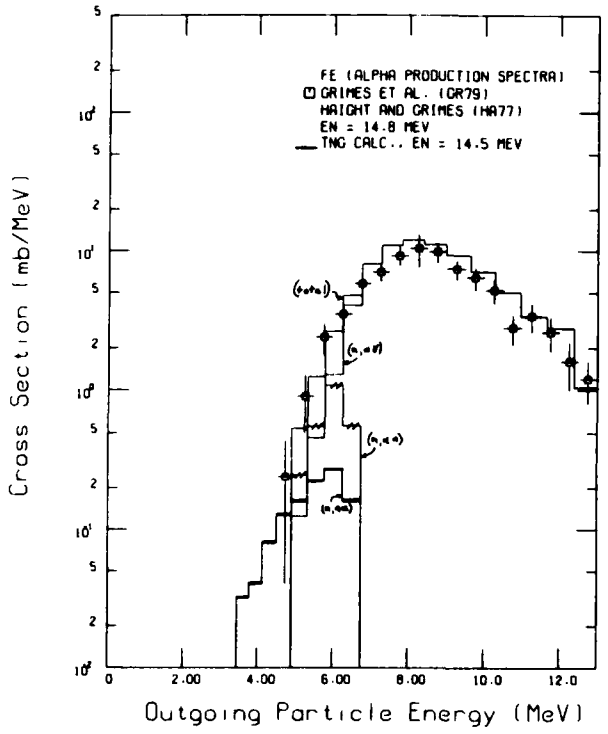

Fig. 9. Comparison of the alpha-particle production spectrum of the present calculation with measurements. Various contributing components in the calculation are shown.

4. FORMAT AND OTHER ADJUSTMENTS

The calculated energy-angle correlations in inelastically scattered neutrons can be accurately represented using the ENDF/B-VI format, a format we have already used for ^{63}Cu and ^{65}Cu (HE84). However, because a general capability in the processing of the ENDF/B-VI evaluations have not been fully developed and because there is a need for immediate application of the present revision of the iron cross-section set, we generated an interim file employing the ENDF/B-V format. The technique used to achieve this goal is discussed. In addition, changes in other cross sections due to the impact of the revised inelastic and $(n,2n)$ cross sections are also described.

The ENDF/B-V Mod-3 cross-section file of iron contains 40 discrete inelastic levels up to 4.510 MeV and a continuum above this energy. For E_n between 4.586 MeV (the threshold of the highest-energy discrete level) and 20 MeV, the file has 40 angular distributions (MT = 51 - 90) for the discrete region and 1 angular distribution (MT = 91) for the continuum. Thus, the energy-angle correlation in the inelastically scattered neutrons is and can only be accurately described for the discrete region in the ENDF/B-V format. The single angular distribution allowed for the continuum cannot possibly be adequate for the wide E_n range between 4.586 and 20 MeV. The obvious solution then is to increase the discrete region and reduce the continuum region. But this solution can cause serious errors and should be used cautiously, as described below.

The first step is to combine some of the existing discrete levels in order to free part of the 40 allowed discrete levels. A good choice of the combination scheme, shown in Table 1, is to sum the cross sections of the discrete levels having threshold energies within a Vitamin-E (WE79) group, thus freeing 17 MT designators for the continuum. Then the old continuum can be simulated by 17 discrete "bins" plus a new continuum having much higher threshold than the old one. The old continuum is now represented by up to 18 angular distributions instead of by a single one; the old discrete region still has 23 angular distributions, probably more than adequate for any applications. As indicated in Table 1, the cross sections of levels having $2.565 \leqslant |Q| \leqslant 3.122$ have been summed but have not been changed; corresponding angular distributions of the new levels are weighted sums of the old ones. Cross sections and angular distributions having $|Q| \geqslant 3.368$ have been replaced by the new calculation. Thus, precisely speaking, the present revision for the inelastic cross section starts at $E_n = 3.428$ MeV, the threshold for exciting the 3.368-MeV level, though the grouping of lower energy levels may have a small effect. The effect would be minimized if the cross sections are processed into the Vitamin-E group structure. Calculated cross sections for the new MT = 70 - 91 have been multiplied by 0.94 to account for the overall effects of (1) the existing inelastic levels of $^{54, 56, 57, 58}$Fe, and (2) the small cross sections of (n,d), (n,t), and $(n,^3\text{He})$ not explicitly included in the calculation.

Next, we consider the choice for the bin width for the new MT = 74 - 90 which is part of the old continuum. The optimum choice for the bin width depends on the energy range of dominance of the inelastic cross section, the accuracy in representing the energy distribution for low E_n, and the accuracy in representing the angular distributions for high E_n. Because the inelastic cross section remains the largest reaction cross section up to E_n = 15 MeV (above which $(n,2n)$ cross section is greater) and because the DT neutron source is near 15 MeV, we

Table 1. Groupings of ENDF/B-V Mod-3 discrete-level inelastic scattering cross sections (MT's) according to the Vitamin-E 174-group structure

Vitamin-E group	Upper energy (MeV)	ENDF/B-V MT's	New MT	Comment
40	2.7253	67-68	67	from ENDF/B-V
38	3.0119	69-70	68	
36	3.3287	71-72	69	
35	3.6788	73-78	70	new calculations
34	4.0675	79-81	71	
33	4.4933	82-88	72	
32	4.7237	89-90	73	

should perhaps represent the energy-angle correlations of the inelastically scattered neutrons accurately for $E_n \leq 15$ MeV. Consequently, a bin width of 0.5 MeV was chosen. The 17 discrete "bins" would push the new continuum Q-value to 13 MeV. For $E_n = 15$ MeV, the continuum width is 2 MeV wide and a single angular distribution representing that of the average E_n' can adequately describe the resulting low-energy outgoing neutrons. For $E_n > 15$ MeV, the continuum energy range is broader, and the angular distribution representing that of the average E_n' for the continuum will again become inadequate. For $E_n < 10$ MeV, the bin width of 0.5 MeV is wider than those of the Vitamin-E groups, some inaccuracies in the energy distribution may result. Therefore, the present method of representing the energy-angle correlations of inelastically scattered neutrons in the ENDF/B-V format cannot replace the ENDF/B-VI format. The present calculated results should be transformed into the ENDF/B-VI format.

The angular distributions for the secondary neutrons in $(n,2n)$, (n,np), and $(n,n\alpha)$ reactions are treated the same way as in the (n,n') continuum. That is, the calculated angular distribution corresponding to that of the average E_n' for each E_n is used. Because, for a given E_n, the average E_n' for $(n,2n)$, (n,np), and $(n,n\alpha)$ are smaller than that for the new (n,n') continuum, the angular distributions for these three reactions tend to be less of a problem.

Now we turn to the impact of the revised inelastic and $(n,2n)$ cross sections on other cross sections. The revised (n,n') and $(n,2n)$ cross sections lead to a reduced nonelastic cross section as shown in Fig. 4. This in turn calls for a reduction in the total cross section, or an increase in the elastic cross section, or both. From the data and the ENDF/B-V values shown in GA76, it can be seen that the total cross section can be reduced 3% from 4.5 to 8 MeV, 2% from 8 to 10 MeV, and 1% from 10 to 12 MeV without worsening the agreement between the evaluated

values and the data. These reductions are adopted for the present revision and result in an increase in the elastic cross section from ENDF/B-V Mod-1 of approximately 3% at 8 MeV to 5% at 15 MeV. The corresponding increase in the elastic cross section from ENDF/B-V Mod-3 is still 3% at 8 MeV but is less than 1% above 13 MeV because the $(n,2n)$ cross section is different between Mod-1 and Mod-3. The gamma-ray production cross section (MF = 13, MT = 3) is reduced in proportion to the reduction in the nonelastic cross section (MT = 3) to approximately conserve energy. The uncertainty file for the inelastic cross section, strongly correlated with the nonelastic cross section, is derived from the uncertainties in the nonelastic cross section and other partial reaction cross sections. The uncertainties in the nonelastic cross section in ENDF/B-V and in the present revision are listed in Table 2. The derived uncertainties for the inelastic cross section are essentially the same as those for the nonelastic cross section in the energy range from threshold to 11 MeV, and are slightly greater than those for the nonelastic cross section at higher energies. The smaller energy groups for the fully-correlated uncertainties in the present case shown in Table 2 will allow integral studies of the type performed by Maerker *et al.* (MA85) to better pin-point problem areas in the cross sections. The uncertainties for MT = 67 - 91, whose cross sections have new definitions, are re-evaluated. These uncertainty files are assumed uncorrelated and each has two components. One component is 10% in broad energy groups (LB = 1), the other is 1% of the peak cross section in absolute magnitude for the entire energy range (LB = 0). The uncertainties of the $(n,2n)$ cross section still seem reasonable and have not been changed.

Table 2. Estimated uncertainties of the nonelastic cross section in ENDF/B-V Mod-3 and in the present revision

ENDF/B-V Mod-3		Present revision	
E_n (MeV)	Uncertainty	E_n (MeV)	Uncertainty
0.8611 - 20	30 MB	0.8611 - 20	30 MB
0.8611 - 3	5%	0.8611 - 2	5%
3 - 8	5%	2 - 4	5%
8 - 14	5%	4 - 6	5%
14 - 20	5%	6 - 8	6%
		8 - 10	7%
		10 - 12	6%
		12 - 14	5%
		14 - 16	5%
		16 - 18	7%
		18 - 20	8%

5. CONCLUSION

The inelastic cross section of iron in ENDF/B-V Mod-3 have been reduced by an average 8% from 3 to 8 MeV and 3% from 8 to 20 MeV. The $(n,2n)$ cross section has been changed by up to 10% from Mod-1 and up to 3% from Mod-3. Energy-angle correlations in the inelastically scattered neutrons have been introduced through the use of "discretized" continuum bins in the ENDF/B-V format. Anistropic angular distributions for the secondary neutrons in the $(n,2n)$, (n,np), and $(n,n\alpha)$ reactions have also been given. All revisions were based on a combined consideration of microscopic data, integral results, and a consistent nuclear model analysis that also included the nonelastic cross section and the 0.847-MeV gamma-ray production cross section.

ACKNOWLEDGEMENTS

This work was sponsored by the Defense Nuclear Agency under contract with Martin Marietta Energy Systems, Inc. The authors gratefully acknowledge the helpful comments of J. K. Dickens and D. T. Ingersoll, and the pleasant cooperation of A. C. Alford in typing several extensive revisions of this report.

REFERENCES

AR80 E. D. Arthur and P. G. Young, *Evaluated Neutron-Induced Cross Sections for $^{54,56}Fe$ to 40 MeV*, LA-8626-MS (ENDF-304), Los Alamos Scientific Laboratory, 1980.

AS58 V. J. Ashby, H. C. Catron, and L. L. Newkirk, *Phys. Rev.* **111**, 616 (1958).

BE56 J. R. Beyster, M. Walt, and E. W. Salmi, *Phys. Rev.* **104**, 1319 (1956).

BE66 R. W. Benjamin, P. S. Buchanan, and I. L. Morgan, *Nucl. Phys.* **79**, 241 (1966).

BE75 Besotosnyj, Gorbachev, Suvorov, and Shretsov, *Jadernye Konstanty* – 19, 77 (1975).

BR67 D. L. Broder, A. G. Dovbenko, V. E. Kolesov, A. I. Lashuk, and I. P. Sadokhin, *Bull. Acad. Sci.* USSR, Phl, 327 (1967).

BR70 D. L. Broder, A. F. Gamalij, A. I. Lashuk, and I. P. Sadokhin, *Second IAEA Conference on Nuclear Data for Reactors*, Helsinki, Finland, June 15-19, 1970.

CH74 V. K. Chuk, G. A. Prokopez and B. Holmqvist, *Sov. J. Nucl. Phys.* *20*(6), 1096 (1974).

CL72 G. Clayeux and J. Voignier, Centre d'Etudes de Limeil CEA-R-4279 (1972).

CO78 V. Corcalciuc, B. Holmqvist, A. Marcinkowski, and G. A. Prokopets, *Nucl. Phys.* **A307**, (3), 445 (1978).

CR76 S. N. Cramer and E. M. Oblow, *Analysis of a Neutron Scattering Integral Experiment on Iron for Neutron Energies from 1 to 15 MeV*, ORNL/TM-5548, Oak Ridge National Laboratory, 1976.

DE61 J. G. Degtjarev and V. G. Nadtochij, *Sov. At. Energy* **11**(4), 397 (1961).

DI72 J. K. Dickens, G. L. Morgan, and F. G. Perey, *Gamma-Ray Production Due to Neutron Interactions with Iron for Incident Neutron Energies Between 0.8 and 20 MeV: Tabulated Differential Cross Sections*, ORNL-4798, Oak Ridge National Laboratory, 1972.

FL56 N. N. Flerov and V. M. Talysin, *Sov. At. Energy* **1**(4), 155, (1956).

FR80 J. Frehaut, A. Bertin, R. Bois, and J. Jary, *Symp. on Neutron Cross Sections from 10-50 MeV*, Brookhaven National Laboratory, May 12-14, 1980.

FU75 C. Y. Fu, "A Two-Step Hauser-Feshbach Model Code with Precompound Effects and Gamma-Ray Cascades - A Tool for Cross Section Evaluation," p. 328 in *Proc. Conf. Nucl. Cross Sections and Technology*, National Bureau of Standards Special Publication SP-425, 1975.

FU76 C. Y. Fu, *Atom. Data Nucl. Data Tables* **17**, 127 (1976).

FU79 C. Y. Fu, "A Consistent Nuclear Model for Compound and Precompound Reactions with Conservation of Angular Momentum," *Proc. Int. Conf. Nuclear Cross Sections for Technology*, National Bureau of Standards Special Publication 593, p. 757, 1979. See also ORNL/TM-7042, Oak Ridge National Laboratory, 1980.

FU80 C. Y. Fu and F. G. Perey, *Evaluation of Neutron and Gamma-Ray Production Cross Sections for Natural Iron (ENDF/B-V MAT 1326)*, ORNL/TM-7523 (ENDF-302), Oak Ridge National Laboratory, 1980.

FU81 C. Y. Fu, "Development and Applications of Multi-Step Hauser-Feshbach/Pre- equilibrium Model Theory," p. 35 in *Nuclear Theory for Applications 1980*, IAEA-SMR-68/1, International Centre for Theoretical Physics, Trieste, 1981.

FU82 C. Y. Fu, *Summary of ENDF/B-V Evaluations for Carbon, Calcium, Iron, Copper, and Lead and ENDF/B-V Mod-3 for Calcium and Iron*, ORNL/TM-8283 (ENDF-325), Oak Ridge National Laboratory, 1982.

FU84 C. Y. Fu, *Nucl. Sci. Eng.* **86**, 344 (1984).

FU85 C. Y. Fu and D. T. Ingersoll, *Trans. Am. Nucl. Soc.* **50**, 470 (1985).

FU86 C. Y. Fu, *Nucl. Sci. Eng.* 92, 440 (1986).

FU87 C. Y. Fu, K. Shibata, and D. M. Hetrick, to be published in 1987.

GA76 D. I. Garber and .R. R. Kinney, "Neutron Cross Sections, Volume II, Curves," BNL-325, Brookhaven National Laboratory, 1976.

GR53 E. R. Graves and L. Rosen, *Phys. Rev.*, **89**, 343 (1953).

GR79 S. M. Grimes, R. C. Haight, K. R. Alvar, H. H. Barschall, and R. R. Borchers, *Phys. Rev.* **C19**, 2127 (1979).

HA77 R. C. Haight and S. M. Grimes, LLL Report UCRL-80235 (1977).

HE75 D. Hermsdorf et al., *Differential Neutron Emission Cross Sections from Iron by 14.6-MeV Neutrons*, ZfK-277, Institute of Nuclear Physics, University of Dresden (East Germany), 1975.

HE84 D. M. Hetrick, C. Y. Fu, and D. C. Larson, "Calculated Neutron-Induced Cross Sections for ^{63,65}Cu from 1 to 20 MeV and comparisons with Experiments," ORNL/TM-9083 (ENDF-337), Oak Ridge National Laboratory, 1984.

JO75 R. H. Johnson, J. J. Dorning, and B. W. Wehring, *Trans. Am. Nucl. Soc.* **22** 799 (1975).

KA72 J. L. Kammerdiener, *Neutron Spectra Emitted by ^{239}Pu, ^{238}U, ^{235}U, Pb, Nb, Ni, Fe, Al, and C Irradiated by 14 MeV Neutrons*, UCRL-51232, Lawrence Livermore Laboratory, 1972.

LA74 J. Lachkar, J. Sigand, Y. Patin, and G. Haouat, *Nucl. Sci. Eng.* **55**, 168 (1974).

LA85 D. C. Larson, "High-Resolution Structural Material (n,$x\gamma$) Production Cross Sections for E_n from 0.2 to 40 MeV," *Int. Conf. Nucl. Data for Basic and Applied Sciences*, Santa Fe, May 13-17, 1975.

LE58 P. P. Lebedev, Y. A. Zisin, Y. S. Klintsov, and B. D. Stsiboiskii, *Sov. At. Energy* **5**(5), 522 (1958).

MA57 M. H. MacGregor, W. P. Ball, and R. Booth, *Phys. Rev.*, **108**, 726 (1957).

MA59 M. K. Machwe, D. W. Kent, Jr., and S. C. Snowdon, *Phys. Rev.* **114**, 1563 (1969).

MA83 A. Marcincowski et al., *Nucl. Sci. Eng.* **83**, 13 (1983).

MA85 R. E. Maerker et al., "Combining Integral and Differential Dosimetry Data in an Unfolding Procedure with Application to the Arkansas Nuclear One-Unit 1 Reactor," *Int. Conf. Nucl. Data for Basic and Applied Sciences*, Santa Fe, May 13-17, 1985.

OR75 V. G. Orphan, C. G. Hoot, and V. C. Rogers, *Nucl. Sci. Eng.*, **57**, 309 (1975).

PA55 M. V. Pasechnik, First UN Conf. on Peaceful Uses of Atomic Energy, Geneva, Aug. 8-20, 1955.

PA85 J. V. Pace, Oak Ridge National Laboratory, Private Communication, 1985.

PH52 D. D. Phillips, R. W. Davis, and E. R. Graves, *Phys. Rev.* **88**, 600 (1952).

QA77 S. M. Qaim and N. I. Molla, *Nucl. Phys.* **A283**, 269 (1977).

RO68 J. Roturier, "Differential Elastic Neutron Cross Sections, Inelastic and Gamma Emission Cross Sections for many Light Elements Tabulated," Thesis, Bordeaux, University. (1968).

SA72 O. A. Salnikov, G. N. Lovchikova, G. V. Kotelnikova, A. M. Trufanov, and N. I. Fetisov, *Jadernye Konstanty* - 7, 102 (1972).

ST57 V. I. Strizhak, *Sov. At. Energy* **2**(1), 68 (1957).

TA55 H. L. Taylor, O. Lonsjo, and T. W. Bonner, *Phys. Rev.* **100**, 174 (1955).

TA83 A. Takahaski et al., *Double Differential Neutron Emission Cross Sections, Numerical Tables and Figures (1983),* A-83-01, Intense 14-MeV Neutron Source Facility, Osaka University, 1983.

TH63 D. B. Thomson, *Phys. Rev.* **129**, 1649 (1963).

VE79 L. R. Veeser, Figure 61 in "Evaluated Neutron-Induced Cross Sections for ^{54,56}Fe to 40 MeV," by E. D. Arthur and P. G. Young, LA-8626-MS (ENDF-304) (1980).

WE62 R. Wenusch and H. Vonach, *Anz. Oesterr. Akad. Wiss., Math - Naturwiss. Kl.* **99**, 1 (1962).

WE79 C. R. Weisbin et al., "Vitamin-E: An ENDF/B-V Multigroup Cross-Section Library for LMFBR Core and Shield, LWR Shield, Dosimetry and Fusion Blanket Technology," ORNL-5505 (ENDF-274), Oak Ridge National Laboratory, 1979.

ORNL/TM-9964
ENDF-341

INTERNAL DISTRIBUTION

1. L. S. Abbott
2. R. G. Alsmiller, Jr.
3. D. G. Cacuci
4. J. K. Dickens
5. P. W. Dickson, Jr. (Consultant)
6-10. C. Y. Fu
11. G. H. Golub (Consultant)
12. R. M. Haralick (Consultant)
13-17. D. M. Hetrick
18. D. T. Ingersoll
19. D. C. Larson
20. R. E. Maerker
21. F. C. Maienschein
22. B. F. Maskewitz
23. J. V. Pace III
24. R. W. Peelle
25. F. G. Perey
26. R. W. Roussin
27. R. T. Santoro
28. D. Steiner (Consultant)
29. A. Zucker
30. Central Research Library Document Reference Section
31. K-25 Plant Library
32-33. Laboratory Records Department
34. ORNL Patent Office
35. Laboratory Records (RC)

EXTERNAL DISTRIBUTION

36. E. D. Arthur, T-2, MS243, Los Alamos National Laboratory, P.O. Box 1663, Los Alamos, NM 87545.
37. S. E. Berk, G234, Division of Development and Technology Office of Fusion Energy, USDOE, Washington, DC 20545.
38. M. R. Bhat, Building 107D, National Nuclear Data Center, Brookhaven National Laboratory, Upton, NY 11973.
39. Chief, Mathematics and Geoscience Branch, DOE, Washington, DC 20545.
40. Herbert Goldstein, 211 Mudd Columbia University, 520 West 120th St., New York, NY 10027.
41. R. C. Haight, P. O. Box 808, L-405, Lawrence Livermore National Laboratory, Livermore, CA 94550.
42. Robert MacFarlane, T-2 MS243, Los Alamos National Laboratory, P. O. Box 1663, Los Alamos, NM 87545.
43. F. M. Mann, W/A-4, Westinghouse Hanford, P. O. Boz 1970, Richland, WA 99352.
44. Robert Schenter, Westinghouse Hanford, P. O. Box 1970, Richland, WA 99352.
45. D. L. Smith, Building 314, Applied Physics Division, Argonne National Laboratory, 9700 South Cass Avenue, Argonne, IL 60439.

46. Stanley Whetstone, Division Nuclear Sciences, Office of Basic Energy Sciences, U. S. DOE, Washington, DC 20545.

47. Phillip Young, T-2, MS-243, Los Alamos National Laboratory, P. O. Box 1663, Los Alamos, NM 87545.

48. Office of Assistant Manager for Energy Research and Development, Department of Energy, Oak Ridge Operations, Oak Ridge, TN 37830.

49-138. April Donegain, National Nuclear Data Center, ENDF, Brookhaven National Laboratory, Upton, NY 11973.

139-165. Technical Information Center, Oak Ridge, TN 37830.

166-400. Defense Nuclear Agency Transport Distribution (AU).

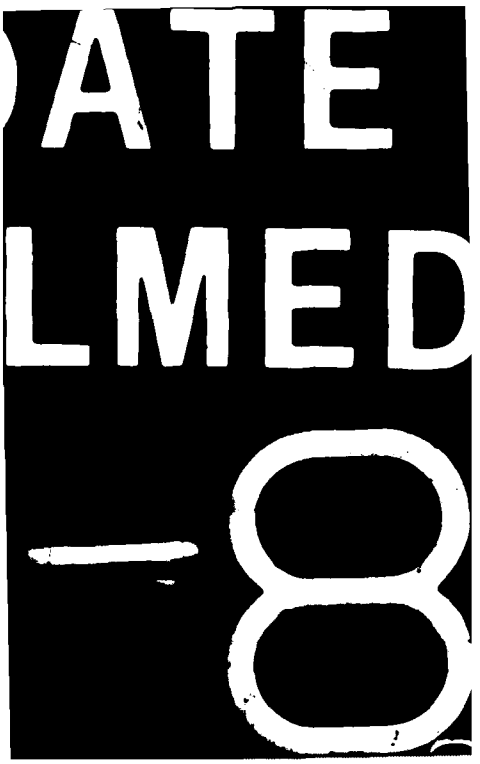
ATE
LMED
8